Engineering Transactions, **68**(3): 269–295, 2020, doi: 10.24423/EngTrans.1187.20200904
Polish Academy of Sciences • Institute of Fundamental Technological Research (IPPT PAN)
Université de Lorraine • Poznan University of Technology

Research Paper

Static Stability Analysis of Mass Sensors Consisting of Hygro-Thermally Activated Graphene Sheets Using a Nonlocal Strain Gradient Theory

Rajendran SELVAMANI[1)*], Madasamy MAHAVEER SREEJAYAN[1)]
Farzad EBRAHIMI[2)]

[1)] *Department of Mathematics*
Karunya Institute of Technology and Sciences
Coimbatore-641114, Tamil Nadu, India
[*]Corresponding Author e-mail: selvamani@karunya.edu

[2)] *Department of Mechanical Engineering*
Imam Khomieni International University
Qazvin 34148-96818, Iran
e-mail: febrahimy@eng.ikiu.ac.ir

This paper develops a nonlocal strain gradient plate model for buckling analysis of graphene sheets under hygro-thermal environments with mass sensors. For a more accurate analysis of graphene sheets, the proposed theory contains two scale parameters related to the nonlocal and strain gradient effects. The graphene sheet is modeled via a two-variable shear deformation plate theory that does not need shear correction factors. Governing equations of a nonlocal strain gradient graphene sheet on the elastic substrate are derived via Hamilton's principle. Galerkin's method is implemented to solve the governing equations for different boundary conditions. Effects of different factors, such as moisture concentration rise, temperature rise, nonlocal parameter, length scale parameter, nanoparticle mass and geometrical parameters, on buckling characteristics of graphene sheets are examined and presented as dispersion graphs.

Key words: humid-thermal buckling; refined plate theory; graphene sheets; nonlocal strain gradient; mass sensor.

1. Introduction

The 2D atomic crystal-like graphene reveals exceptional electronic and mechanical properties. Many carbon-based nanostructures, including carbon nanotubes, nanoplates and nanobeams, are considered as deformed graphene sheets, see LIM *et al.* [1]. In fact, analysis of graphene sheets is a basic matter in the study of nanomaterials and nanostructures. Analysis of scale-free plates employing classical theories has been presented widely in the literature. However, such theories are not able to examine the scale effects on the nanostructures with small size. Therefore, the nonlocal elasticity theory of Eringen [2–3] was developed taking into account small scale effects. Contrary to the local theory in which the stress state at any given point depends only on the strain state at that point, in the nonlocal theory, the stress state at a given point depends on the strain states at all points. The nonlocal elasticity theory has been broadly applied to investigate the mechanical behavior of nanoscale structures (HASHEMI and SAMAEI [4], KHEROUBI *et al.* [5], EBRAHIMI and DAMAN [6], RAKRAK *et al.* [7], AYDOGDU *et al.* [8], ELMERABET *et al.* [9]).

PRADHAN and MURMU [10] examined nonlocal influences on buckling behavior of a single-layer graphene sheet subjected to uniform in-plane loadings. PRADHAN and KUMAR [11] performed a vibration study of orthotropic graphene sheets incorporating nonlocal effects using a semi-analytical approach. The application of the Levy type method to stability and vibrational investigation of nanosize plates including nonlocal effects was examined by AKSENCER and AYDOGDU [12]. MOHAMMADI *et al.* [13] performed a shear buckling analysis of an orthotropic graphene sheet on an elastic substrate including thermal loading effect. In another work, MOHAMMADI *et al.* [14] examined the effect of in-plane loading on nonlocal vibrational behavior of circular graphene sheets. ANSARI *et al.* [15] explored the vibration response of embedded nonlocal multi-layered graphene sheets accounting for various boundary conditions. SHEN *et al.* [16] studied the vibration behavior of the nanomechanical mass sensor based on the nonlocal graphene sheet model. They showed that the vibration response of the graphene sheet is significantly influenced by the mass of the attached nanoparticle. FARAJPOUR *et al.* [17] examined the static stability of nonlocal plates subjected to non-uniform in-plane edge loads. ANSARI and SAHMANI [18] employed molecular dynamics simulations to examine the biaxial buckling behavior of single-layered graphene sheets based on nonlocal elasticity theory. They matched the results obtained by molecular dynamics simulations with those of the nonlocal plate model to extract the appropriate values of nonlocal parameter. Static bending and vibrational behavior of single-layered graphene sheets on the Winkler-Pasternak foundation based on a two-variable higher- order shear deformation theory were studied by SOBHY [19], EBRAHIMI and BARATI [20], and EHYAEI and DAMAN [21]. NARENDAR and GOPALAKRISHNAN [22] carried out a size-dependent stability analysis of orthotropic nanoscale plates according to a nonlocal two-variable refined plate theory. They stated that the two-variable refined plate model considers the transverse shear influences through the thickness of the plate; hence it is unnecessary to apply shear correction factors. Murmu *et al.* [23] explored the influence of unidirectional magnetic fields on the vibrational behavior of nonlocal single-layer graphene sheets resting on an elastic substrate. Bessaim *et al.* [24] presented a nonlocal quasi-3D trigonometric plate model for the free vibration behavior of micro/nanoscale plates. Hashemi *et al.* [25] studied the free vibrational behavior of double viscoelastic graphene sheets coupled by visco-Pasternak medium. Ebrahimi and Shafiei [26] examined the influence of initial shear stress on the vibration behavior of single-layered graphene sheets embedded in an elastic medium based on Reddy's higher-order shear deformation plate theory. Jiang *et al.* [27] conducted the vibration analysis of a single-layered graphene sheet-based mass sensor using the Galerkin strip distributed transfer function method. Arani *et al.* [28] examined nonlocal vibration of axially moving graphene sheet resting on the orthotropic visco-Pasternak foundation under a longitudinal magnetic field. The thermoelastic bending analysis of carbon nanotube (CNT) and functionally graded carbon nanotube (FG CNT) was illustrated and the hygro-thermal activity was analyzed by different solution methods (Aslanyan and Sargyan [29], Bachiri *et al.* [30], Cinefra *et al.* [31], Jaiani and Bitsadze [32], Khdeir [33], Mirzaei [34], Vinyas *et al.* [35], Kurtinaitiene *et al.* [36], Ebrahimi *et al.* [37], Ebrahimi and Habibi [38]). Sobhy [39] analyzed the hygro-thermal vibrational behavior of coupled graphene sheets by an elastic medium using the two-variable plate theory. Zenkour [40] conducted a transient thermal analysis of graphene sheets on a viscoelastic foundation based on the nonlocal elasticity theory. Aydogdu and Filiz [41] analyzed the modeling carbon nanotube-based mass sensors using axial vibration and nonlocal elasticity. They showed that the axial vibration behavior of single-walled carbon nanotubes can be used in mass sensors. Sakhaee-Pour *et al.* [42] studied the applications of single-layered graphene sheets as mass sensors and atomistic dust detectors.

It is clear that all of the previous papers on graphene sheets applied only the nonlocal elasticity theory to capture small scale effects. However, the nonlocal elasticity theory has some limitations in the accurate prediction of the mechanical behavior of nanostructures. For example, the nonlocal elasticity theory is unable to examine the stiffness increment observed in experimental works and strain gradient elasticity (Lam *et al.* [43]). Recently, Lim *et al.* [1] proposed the nonlocal strain gradient theory to introduce both of the length scales into a single theory. The nonlocal strain gradient theory captures the true influence of the two length scale parameters on the physical and mechanical behavior of small size structures, see Li *et al.* [44]. Ebrahimi and Barati [45–56] applied the nonlocal strain gradient theory to analyze nanobeams. They stated that mechanical characteristics of nanostructures are significantly affected by stiffness-softening and stiffness-hardening mechanisms due to the nonlocal and strain gradient effects, respectively. Ebrahimi *et al.* [57] analyzed the thermal buckling analysis of the magneto-electro-elastic porous FG beam in the thermal environment. Ebrahimi *et al.* [58] developed the bending analysis of the magneto-electro piezoelectric nanobeams system under hygro-thermal loading. Ebrahimi *et al.* [59] studied the dynamic characteristics of hygro-magneto-thermo-electrical nanobeam with non-ideal boundary conditions. Ebrahimi [60] studied the thermo-electro-elastic nonlinear stability analysis of viscoelastic double-piezo nanoplates under the magnetic field. Selvamani and Ebrahimi [61] investigated the axisymmetric vibration in a submerged, piezoelectric rod coated with a thin film. Most recently, Ebrahimi and Salari [62] extended the nonlocal strain gradient theory to analyze nanoplates to obtain the wave frequencies for a range of two scale parameters. So, it is crucial to incorporate both nonlocal and strain gradient effects in the initial analysis of graphene sheets.

Based on the newly developed nonlocal strain gradient theory, buckling behavior of single-layer graphene sheets-based mass sensors in hygro-thermal environment resting on the elastic medium is examined in this paper using a refined two-variable plate theory. The theory introduces two scale parameters corresponding to nonlocal and strain gradient effects to capture both stiffness-softening and stiffness-hardening influences. Hamilton's principle is employed to obtain the governing equation of a nonlocal strain gradient graphene sheet. These equations are solved via Galerkin's method to obtain the natural frequencies. It is shown that the buckling behavior of graphene sheets is significantly influenced by the nonlocal parameter, length scale parameter, moisture concentration rise, nanoparticle mass, orthotropic elastic foundation and boundary conditions.

2. Problem formulation

The higher-order refined plate theory has the following displacement field:

$$u_1(x,y,z) = u(x,y) - z\frac{\partial w_b}{\partial x} - f(z)\frac{\partial w_s}{\partial x}, \tag{2.1}$$

$$u_2(x,y,z) = v(x,y) - z\frac{\partial w_b}{\partial y} - f(z)\frac{\partial w_s}{\partial y}, \tag{2.2}$$

$$u_3(x,y,z) = w_b(x,y) + w_s(x,y), \tag{2.3}$$

where the present theory has a trigonometric function in the following form:

$$f(z) = z - \frac{h}{\pi}\sin\left(\frac{\pi z}{h}\right). \tag{2.4}$$

Also, u and v are displacements components of the mid-surface and w_b and w_s denote the bending and shear transverse displacement, respectively. Nonzero strains of present plate model are expressed as follows:

$$\begin{Bmatrix} \varepsilon_x \\ \varepsilon_y \\ \gamma_{xy} \end{Bmatrix} = +z \begin{Bmatrix} \kappa_x^b \\ \kappa_y^b \\ \kappa_{xy}^b \end{Bmatrix} + f(z) \begin{Bmatrix} \kappa_x^s \\ \kappa_y^s \\ \kappa_{xy}^s \end{Bmatrix}, \tag{2.5}$$

$$\begin{Bmatrix} \gamma_{yz} \\ \gamma_{xz} \end{Bmatrix} = g(z) \begin{Bmatrix} \gamma_{yz}^s \\ \gamma_{xz}^s \end{Bmatrix},$$

where $g(z) = 1 - \mathrm{d}f/\mathrm{d}z$ and

$$\begin{Bmatrix} \kappa_x^b \\ \kappa_y^b \\ \kappa_{xy}^b \end{Bmatrix} = \begin{Bmatrix} -\dfrac{\partial^2 w_b}{\partial x^2} \\ -\dfrac{\partial^2 w_b}{\partial y^2} \\ -2\dfrac{\partial^2 w_b}{\partial x \partial y} \end{Bmatrix}, \qquad \begin{Bmatrix} \kappa_x^s \\ \kappa_y^s \\ \kappa_{xy}^s \end{Bmatrix} = \begin{Bmatrix} -\dfrac{\partial^2 w_s}{\partial x^2} \\ -\dfrac{\partial^2 w_s}{\partial y^2} \\ -2\dfrac{\partial^2 w_s}{\partial x \partial y} \end{Bmatrix}, \tag{2.6}$$

$$\begin{Bmatrix} \gamma_{yz}^s \\ \gamma_{xz}^s \end{Bmatrix} = \begin{Bmatrix} \dfrac{\partial w_s}{\partial y} \\ \dfrac{\partial w_s}{\partial x} \end{Bmatrix}.$$

Also, Hamilton's principle expresses that

$$\int_0^t \delta(U+V)\,\mathrm{d}t = 0 \tag{2.7}$$

in which U is strain energy and V is work done by external loads. The variation of strain energy is calculated as

$$\delta U = \int_v \sigma_{ij}\delta\varepsilon_{ij}\,\mathrm{d}V = \int_v (\sigma_x\delta\varepsilon_x + \sigma_y\delta\varepsilon_y + \sigma_{xy}\delta\gamma_{xy} + \sigma_{yz}\delta\gamma_{yz} + \sigma_{xz}\delta\gamma_{xz})\,\mathrm{d}V. \tag{2.8}$$

Substituting Eqs (2.5) and (2.6) into Eq. (2.8) yields:

$$\delta U=\int_0^b\int_0^a\Bigg[-M_x^b\frac{\partial^2\delta w_b}{\partial x^2}-M_x^s\frac{\partial^2\delta w_s}{\partial x^2}-M_y^b\frac{\partial^2\delta w_b}{\partial y^2}-M_y^s\frac{\partial^2\delta w_s}{\partial y^2}$$
$$-2M_{xy}^b\frac{\partial^2\delta w_b}{\partial x\partial y}-2M_{xy}^s\frac{\partial^2\delta w_s}{\partial x\partial y}+Q_{yz}\frac{\partial\delta w_s}{\partial y}+Q_{xz}\frac{\partial\delta w_s}{\partial x}\Bigg]\,\mathrm{d}x\,\mathrm{d}y \tag{2.9}$$

in which

$$\left(M_i^b,M_i^s\right)=\int_{-h/2}^{h/2}(z,f)\,\sigma_i\,\mathrm{d}z,\quad i=(x,y,xy),$$
$$Q_i=\int_{-h/2}^{h/2}g\sigma_i\,\mathrm{d}z,\quad i=(xz,yz). \tag{2.10}$$

The variation of the work done by applied loads can be written as

$$\delta V=\int_0^b\int_0^a\Bigg(N_x^0\frac{\partial(w_b+w_s)}{\partial x}\frac{\partial\delta(w_b+w_s)}{\partial x}+N_y^0\frac{\partial(w_b+w_s)}{\partial y}\frac{\partial\delta(w_b+w_s)}{\partial y}$$
$$+2\delta N_{xy}^0\frac{\partial(w_b+w_s)}{\partial x}\frac{\partial(w_b+w_s)}{\partial y}-k_w\delta(w_b+w_s)+q_{\text{particle}}\delta(w_b+w_s)$$
$$+k_p\left(\frac{\partial(w_b+w_s)}{\partial x}\frac{\partial\delta(w_b+w_s)}{\partial x}+\frac{\partial(w_b+w_s)}{\partial y}\frac{\partial\delta(w_b+w_s)}{\partial y}\right)\Bigg)\,\mathrm{d}x\,\mathrm{d}y, \tag{2.11$_1$}$$

where N_x^0, N_y^0, N_{xy}^0 are in-plane applied loads, and k_w and k_p are the Winkler and Pasternak constants. Also, q_{particle} is the transverse force due to attached nanoparticles (such as a buckyball and molecular or bacterium) with mass m_c attached at the location $x=x_0$, $y=y_0$:

$$q_{\text{particle}}=-\sum_{j=1}^N m_j\delta(x-x_j,y-y_j)\frac{\partial^2 w}{\partial t^2}, \tag{2.11$_2$}$$

in which m_j is the mass of j-th attached particle and N is the number of concentrated masses. Also, $\delta(x-x_j)$ is the Dirac delta function defined by:

$$\delta(x-x_j)=\begin{cases}\infty & \text{for}\quad x\neq x_j,\\ 0 & \text{for}\quad x=x_j.\end{cases} \tag{2.11$_3$}$$

By inserting Eqs (2.8)–(2.11) into Eq. (2.7) and setting the coefficients of δw_b and δw_s to zero, the following Euler-Lagrange equations can be obtained:

$$\begin{aligned}(2.12)\quad & \frac{\partial^2 M_x^b}{\partial x^2}+2\frac{\partial^2 M_{xy}^b}{\partial x\partial y}+\frac{\partial^2 M_y^b}{\partial y^2}-(N^T+N^H)\nabla^2(w_b+w_s)\\ &+k_p\left[\frac{\partial^2(w_b+w_s)}{\partial x^2}+\frac{\partial^2(w_b+w_s)}{\partial y^2}\right]-k_w(w_b+w_s)\\ &-\sum_{j=1}^{N} m_j\delta(x-x_j,y-y_j)\frac{\partial^2 w}{\partial t^2}=0,\end{aligned}$$

$$\begin{aligned}(2.13)\quad & \frac{\partial^2 M_x^s}{\partial x^2}+2\frac{\partial^2 M_{xy}^s}{\partial x\partial y}+\frac{\partial^2 M_y^s}{\partial y^2}+\frac{\partial Q_{xz}}{\partial x}+\frac{\partial Q_{yz}}{\partial y}-(N^T+N^H)\nabla^2(w_b+w_s)\\ &+k_p\left[\frac{\partial^2(w_b+w_s)}{\partial x^2}+\frac{\partial^2(w_b+w_s)}{\partial y^2}\right]-k_w(w_b+w_s)\\ &-\sum_{j=1}^{N} m_j\delta(x-x_j,y-y_j)\frac{\partial^2 w}{\partial t^2}=0,\end{aligned}$$

where $N_x^0=N_y^0=N^T+N^H$, $N_{xy}^0=0$, and hygro-thermal resultant can be expressed as

$$N^T=\int\limits_{-h/2}^{h/2}\frac{E}{1-v}\alpha\Delta T\,\mathrm{d}z, \tag{2.14}$$

$$N^H=\int\limits_{-h/2}^{h/2}\frac{E}{1-v}\beta\Delta C\,\mathrm{d}z. \tag{2.15}$$

2.1. Strain gradient nanoplate model via nonlocal form

The newly developed nonlocal strain gradient theory [37] takes into account both the nonlocal stress field and the strain gradient effects by introducing two scale parameters. This theory defines the stress field as

$$\sigma_{ij}=\sigma_{ij}^{(0)}-\frac{\mathrm{d}\sigma_{ij}^{(1)}}{\mathrm{d}x}, \tag{2.16}$$

in which the stresses $\sigma_{xx}^{(0)}$ and $\sigma_{xx}^{(1)}$ are corresponding to strain ε_{xx} and strain gradient $\varepsilon_{xx,x}$, respectively as

$$\sigma_{ij}^{(0)} = \int_0^L C_{ijkl}\,\alpha_0(x,x',e_0a)\varepsilon'_{kl}(x')\,\mathrm{d}x',$$
(2.17)
$$\sigma_{ij}^{(1)} = l^2\int_0^L C_{ijkl}\,\alpha_1(x,x',e_1a)\varepsilon'_{kl,x}(x')\,\mathrm{d}x',$$

in which C_{ijkl} are the elastic coefficients, e_0a and e_1a capture the nonlocal effects and l captures the strain gradient effects. When the nonlocal functions $\alpha_0(x,x',e_0a)$ and $\alpha_1(x,x',e_1a)$ satisfy the developed conditions by ERINGEN [3], the constitutive relation of nonlocal strain gradient theory has the following form:

$$[1-(e_1a)^2\nabla^2][1-(e_0a)^2\nabla^2]\sigma_{ij} = C_{ijkl}[1-(e_1a)^2\nabla^2]\varepsilon_{kl} - C_{ijkl}l^2[1-(e_0a)^2\nabla^2]\nabla^2\varepsilon_{kl}, \tag{2.18}$$

in which ∇^2 denotes the Laplacian operator. Considering $e_1 = e_0 = e$, the general constitutive relation in Eq. (2.18) becomes:

$$[1-(ea)^2\nabla^2]\sigma_{ij} = C_{ijkl}[1-l^2\nabla^2]\varepsilon_{kl}. \tag{2.19}$$

To consider hygro-thermal effects, Eq. (2.19) can be written as [35]

$$[1-(ea)^2\nabla^2]\sigma_{ij} = C_{ijkl}[1-l^2\nabla^2](\varepsilon_{kl}-\alpha_{kl}T-\beta_{kl}C), \tag{2.20}$$

where α_{kl} and β_{kl} are thermal and moisture expansion coefficients, respectively. Finally, the constitutive relations of nonlocal strain gradient theory can be expressed by:

$$(1-(ea)^2\nabla^2)\begin{Bmatrix}\sigma_x\\ \sigma_y\\ \sigma_{xy}\\ \sigma_{yz}\\ \sigma_{xz}\end{Bmatrix} = (1-l^2\nabla^2) \cdot \begin{pmatrix} Q_{11} & Q_{12} & 0 & 0 & 0\\ Q_{12} & Q_{22} & 0 & 0 & 0\\ 0 & 0 & Q_{66} & 0 & 0\\ 0 & 0 & 0 & Q_{44} & 0\\ 0 & 0 & 0 & 0 & Q_{55}\end{pmatrix}\begin{Bmatrix}\varepsilon_x-\alpha\Delta T-\beta\Delta C\\ \varepsilon_y-\alpha\Delta T-\beta\Delta C\\ \gamma_{xy}\\ \gamma_{yz}\\ \gamma_{xz}\end{Bmatrix}, \tag{2.21}$$

where

$$Q_{11}=Q_{22}=\frac{E}{1-\upsilon^2},\quad Q_{12}=\upsilon Q_{11},\quad Q_{44}=Q_{55}=Q_{66}=\frac{E}{2(1+\upsilon)}. \tag{2.22}$$

Inserting Eq. (2.10) in Eq. (2.23) gives:

$$\begin{aligned}\big(1-(ea)^2\nabla^2\big)\begin{Bmatrix} M_x^b \\ M_y^b \\ M_{xy}^b \end{Bmatrix}=(1-l^2\nabla^2)&\left[\begin{pmatrix} D_{11} & D_{12} & 0 \\ D_{12} & D_{22} & 0 \\ 0 & 0 & D_{66} \end{pmatrix}\begin{Bmatrix} -\dfrac{\partial^2 w_b}{\partial x^2} \\ -\dfrac{\partial^2 w_b}{\partial y^2} \\ -2\dfrac{\partial^2 w_b}{\partial x\partial y} \end{Bmatrix}\right.\\ &\left.+\begin{pmatrix} D_{11}^s & D_{12}^s & 0 \\ D_{12}^s & D_{22}^s & 0 \\ 0 & 0 & D_{66}^s \end{pmatrix}\begin{Bmatrix} -\dfrac{\partial^2 w_s}{\partial x^2} \\ -\dfrac{\partial^2 w_s}{\partial y^2} \\ -2\dfrac{\partial^2 w_s}{\partial x\partial y} \end{Bmatrix}\right],\end{aligned} \tag{2.23}$$

$$\begin{aligned}\big(1-(ea)^2\nabla^2\big)\begin{Bmatrix} M_x^s \\ M_y^s \\ M_{xy}^s \end{Bmatrix}=(1-l^2\nabla^2)&\left[\begin{pmatrix} D_{11}^s & D_{12}^s & 0 \\ D_{12}^s & D_{22}^s & 0 \\ 0 & 0 & D_{66}^s \end{pmatrix}\begin{Bmatrix} -\dfrac{\partial^2 w_b}{\partial x^2} \\ -\dfrac{\partial^2 w_b}{\partial y^2} \\ -2\dfrac{\partial^2 w_b}{\partial x\partial y} \end{Bmatrix}\right.\\ &\left.+\begin{pmatrix} H_{11}^s & H_{12}^s & 0 \\ H_{12}^s & H_{22}^s & 0 \\ 0 & 0 & H_{66}^s \end{pmatrix}\begin{Bmatrix} -\dfrac{\partial^2 w_s}{\partial x^2} \\ -\dfrac{\partial^2 w_s}{\partial y^2} \\ -2\dfrac{\partial^2 w_s}{\partial x\partial y} \end{Bmatrix}\right],\end{aligned} \tag{2.24}$$

$$\big(1-(ea)^2\nabla^2\big)\begin{Bmatrix} Q_x \\ Q_y \end{Bmatrix}=(1-l^2\nabla^2)\left[\begin{pmatrix} A_{44}^s & 0 \\ 0 & A_{55}^s \end{pmatrix}\begin{Bmatrix} \dfrac{\partial w_s}{\partial x} \\ \dfrac{\partial w_s}{\partial y} \end{Bmatrix}\right], \tag{2.25}$$

in which the cross-sectional rigidities are defined as follows:

$$\left\{\begin{array}{c} D_{11}, D_{11}^s, H_{11}^s \\ D_{12}, D_{12}^s, H_{12}^s \\ D_{66}, D_{66}^s, H_{66}^s \end{array}\right\} = \int\limits_{-h/2}^{h/2} Q_{11}(z^2, zf, f^2) \left\{\begin{array}{c} 1 \\ \nu \\ \dfrac{1-\nu}{2} \end{array}\right\} \mathrm{d}z, \tag{2.26}$$

$$A_{44}^s = A_{55}^s = \int\limits_{-h/2}^{h/2} g^2 \frac{E}{2(1+v)}\,\mathrm{d}z. \tag{2.27}$$

The governing equations of the nonlocal strain gradient graphene sheet in terms of the displacement are obtained by inserting Eqs (2.23)–(2.25) into Eqs (2.12) and (2.13) as follows:

$$\begin{aligned}
& - D_{11}\left[\frac{\partial^4 w_b}{\partial x^4} - l^2\left(\frac{\partial^6 w_b}{\partial x^6} + \frac{\partial^6 w_b}{\partial x^4 \partial y^2}\right)\right] \\
&\qquad - 2(D_{12}+2D_{66})\left[\frac{\partial^4 w_b}{\partial x^2 \partial y^2} - l^2\left(\frac{\partial^6 w_b}{\partial x^4 \partial y^2} + \frac{\partial^6 w_b}{\partial x^2 \partial y^4}\right)\right] \\
& - D_{22}\left[\frac{\partial^4 w_b}{\partial y^4} - l^2\left(\frac{\partial^6 w_b}{\partial y^6} + \frac{\partial^6 w_b}{\partial y^4 \partial x^2}\right)\right] - D_{11}^s\left[\frac{\partial^4 w_s}{\partial x^4} - l^2\left(\frac{\partial^6 w_s}{\partial x^6} + \frac{\partial^6 w_s}{\partial x^4 \partial y^2}\right)\right] \\
&\qquad - 2(D_{12}^s + 2D_{66}^s)\left[\frac{\partial^4 w_s}{\partial x^2 \partial y^2} - l^2\left(\frac{\partial^6 w_s}{\partial x^4 \partial y^2} + \frac{\partial^6 w_s}{\partial x^2 \partial y^4}\right)\right] \\
& - D_{22}^s\left[\frac{\partial^4 w_s}{\partial y^4} - l^2\left(\frac{\partial^6 w_s}{\partial y^6} + \frac{\partial^6 w_s}{\partial y^4 \partial x^2}\right)\right] - (N^T+N^H)\left[\frac{\partial^2 (w_b+w_s)}{\partial x^2} + \frac{\partial^2 (w_b+w_s)}{\partial y^2}\right. \\
&\qquad \left. - (ea)^2\left(\frac{\partial^4 (w_b+w_s)}{\partial x^4} + 2\frac{\partial^4 (w_b+w_s)}{\partial x^2 \partial y^2} + \frac{\partial^4 (w_b+w_s)}{\partial y^4}\right)\right] \\
&\qquad + k_p\left[\frac{\partial^2 (w_b+w_s)}{\partial x^2} + \frac{\partial^2 (w_b+w_s)}{\partial y^2}\right. \\
&\qquad \left. - (ea)^2\left(\frac{\partial^4 (w_b+w_s)}{\partial x^4} + 2\frac{\partial^4 (w_b+w_s)}{\partial x^2 \partial y^2} + \frac{\partial^4 (w_b+w_s)}{\partial y^4}\right)\right] \\
&\qquad - k_w\left[(w_b+w_s) - (ea)^2\left(\frac{\partial^2 (w_b+w_s)}{\partial x^2} + \frac{\partial^2 (w_b+w_s)}{\partial y^2}\right)\right] \\
&\qquad - \sum_{j=1}^{N} m_j \delta(x - x_j, y - y_j)\frac{\partial^2 w}{\partial t^2} = 0,
\end{aligned} \tag{2.28}$$

$$
\begin{aligned}
(2.29)\quad & - D_{11}^s\left[\frac{\partial^4 w_b}{\partial x^4} - l^2\left(\frac{\partial^6 w_b}{\partial x^6} + \frac{\partial^6 w_b}{\partial x^4 \partial y^2}\right)\right] \\
& + A_{55}^s\left[\frac{\partial^2 w_s}{\partial x^2} - l^2\left(\frac{\partial^4 w_s}{\partial x^4} + \frac{\partial^4 w_s}{\partial x^2 \partial y^2}\right)\right] + A_{44}^s\left[\frac{\partial^2 w_s}{\partial y^2} - l^2\left(\frac{\partial^4 w_s}{\partial y^4} + \frac{\partial^4 w_s}{\partial y^2 \partial x^2}\right)\right] \\
& - 2(D_{12}^s + 2D_{66}^s)\left[\frac{\partial^4 w_b}{\partial x^2 \partial y^2} - l^2\left(\frac{\partial^6 w_b}{\partial x^4 \partial y^2} + \frac{\partial^6 w_b}{\partial x^2 \partial y^4}\right)\right] \\
& - D_{22}^s\left[\frac{\partial^4 w_b}{\partial y^4} - l^2\left(\frac{\partial^6 w_b}{\partial y^6} + \frac{\partial^6 w_b}{\partial y^4 \partial x^2}\right)\right] - H_{11}^s\left[\frac{\partial^4 w_s}{\partial x^4} - l^2\left(\frac{\partial^6 w_s}{\partial x^6} + \frac{\partial^6 w_s}{\partial x^4 \partial y^2}\right)\right] \\
& - 2(H_{12}^s + 2H_{66}^s)\left[\frac{\partial^4 w_s}{\partial x^2 \partial y^2} - l^2\left(\frac{\partial^6 w_s}{\partial x^4 \partial y^2} + \frac{\partial^6 w_s}{\partial x^2 \partial y^4}\right)\right] \\
& - H_{22}^s\left[\frac{\partial^4 w_s}{\partial y^4} - l^2\left(\frac{\partial^6 w_s}{\partial y^6} + \frac{\partial^6 w_s}{\partial y^4 \partial x^2}\right)\right] - (N^T + N^H)\left[\frac{\partial^2 (w_b + w_s)}{\partial x^2} + \frac{\partial^2 (w_b + w_s)}{\partial y^2}\right. \\
& \left. - (ea)^2\left(\frac{\partial^4 (w_b + w_s)}{\partial x^4} + 2\frac{\partial^4 (w_b + w_s)}{\partial x^2 \partial y^2} + \frac{\partial^4 (w_b + w_s)}{\partial y^4}\right)\right] \\
& + k_p\left[\frac{\partial^2 (w_b + w_s)}{\partial x^2} + \frac{\partial^2 (w_b + w_s)}{\partial y^2} - (ea)^2\left(\frac{\partial^4 (w_b + w_s)}{\partial x^4}\right.\right. \\
& \left.\left. + 2\frac{\partial^4 (w_b + w_s)}{\partial x^2 \partial y^2} + \frac{\partial^4 (w_b + w_s)}{\partial y^4}\right)\right] \\
& - k_w\left[(w_b + w_s) - (ea)^2\left(\frac{\partial^2 (w_b + w_s)}{\partial x^2} + \frac{\partial^2 (w_b + w_s)}{\partial y^2}\right)\right] \\
& - \sum_{j=1}^{N} m_j \delta(x - x_j, y - y_j)\frac{\partial^2 w}{\partial t^2} = 0.
\end{aligned}
$$

3. Solution by Galerkin's method

In this section, Galerkin's method is implemented to solve the governing equations of nonlocal strain gradient graphene sheets. Thus, the displacement field can be calculated as:

$$
w_b = \sum_{m=1}^{\infty}\sum_{n=1}^{\infty} W_{bmn} \Phi_{bm}(x) \Psi_{bn}(y), \tag{3.1}
$$

$$
w_s = \sum_{m=1}^{\infty}\sum_{n=1}^{\infty} W_{smn} \Phi_{sm}(x) \Psi_{sn}(y), \tag{3.2}
$$

where (W_{bmn}, W_{smn}) are the unknown coefficients and the functions Φ_m and Ψ_n satisfy boundary conditions. Boundary conditions based on present plate model are:

• simply-supported edge:

$$w_b = w_s = 0, \qquad \frac{\partial^2 w_b}{\partial x^2} = \frac{\partial^2 w_s}{\partial x^2} = \frac{\partial^2 w_b}{\partial y^2} = \frac{\partial^2 w_s}{\partial y^2} = 0, \tag{3.3}$$

• clamped edge:

$$w_b = w_s = 0, \qquad \frac{\partial w_b}{\partial x} = \frac{\partial w_s}{\partial x} = \frac{\partial w_b}{\partial y} = \frac{\partial w_s}{\partial y} = 0. \tag{3.4}$$

Inserting Eqs (3.1) and (3.2) into Eqs (2.28) and (2.29) and multiplying both sides of the equations by $\Phi_{im}\Psi_{in}$ $(i = bs)$ and integrating over the whole region leads to the following simultaneous equations:

$$\begin{aligned}
\int_0^b\int_0^a \Phi_{bm}\Psi_{bn}\Bigg[&-D_{11}\left[\frac{\partial^4\Phi_{bm}}{\partial x^4}\Psi_{bn} - l^2\left(\frac{\partial^6\Phi_{bm}}{\partial x^6}\Psi_{bn} + \frac{\partial^4\Phi_{bm}}{\partial x^4}\frac{\partial^2\Psi_{bn}}{\partial y^2}\right)\right]\\
&- 2(D_{12}+2D_{66})\left[\frac{\partial^2\Phi_{bm}}{\partial x^2}\frac{\partial^2\Psi_{bn}}{\partial y^2} - l^2\left(\frac{\partial^4\Phi_{bm}}{\partial x^4}\frac{\partial^2\Psi_{bn}}{\partial y^2} + \frac{\partial^2\Phi_{bm}}{\partial x^2}\frac{\partial^4\Psi_{bn}}{\partial y^4}\right)\right]\\
&- D_{22}\left[\frac{\partial^4\Psi_{bm}}{\partial y^4}\Phi_{bn} - l^2\left(\frac{\partial^6\Psi_{bm}}{\partial y^6}\Phi_{bn} + \frac{\partial^2\Phi_{bm}}{\partial x^2}\frac{\partial^4\Psi_{bn}}{\partial y^4}\right)\right]\\
&- D^s_{11}\left[\frac{\partial^4\Phi_{sm}}{\partial x^4}\Psi_{sn} - l^2\left(\frac{\partial^6\Phi_{sm}}{\partial x^6}\Psi_{sn} + \frac{\partial^4\Phi_{sm}}{\partial x^4}\frac{\partial^2\Psi_{sn}}{\partial y^2}\right)\right]\\
&- 2(D^s_{12}+2D^s_{66})\left[\frac{\partial^2\Phi_{sm}}{\partial x^2}\frac{\partial^2\Psi_{sn}}{\partial y^2} - l^2\left(\frac{\partial^4\Phi_{sm}}{\partial x^4}\frac{\partial^2\Psi_{sn}}{\partial y^2} + \frac{\partial^2\Phi_{sm}}{\partial x^2}\frac{\partial^4\Psi_{sn}}{\partial y^4}\right)\right]\\
&- D^s_{22}\left[\frac{\partial^4\Psi_{sm}}{\partial y^4}\Phi_{sn} - l^2\left(\frac{\partial^6\Psi_{sm}}{\partial y^6}\Phi_{sn} + \frac{\partial^2\Phi_{sm}}{\partial x^2}\frac{\partial^4\Psi_{sn}}{\partial y^4}\right)\right]\\
&- (N^T+N^H)\Bigg[\frac{\partial^2\Phi_{bm}}{\partial x^2}\Psi_{bn} + \frac{\partial^2\Phi_{sm}}{\partial x^2}\Psi_{sn} + \frac{\partial^2\Psi_{sm}}{\partial y^2}\Phi_{sn} + \frac{\partial^2\Psi_{bm}}{\partial y^2}\Phi_{bn}\\
&- (ea)^2\left(\frac{\partial^4\Phi_{bm}}{\partial x^4}\Psi_{bn} + \frac{\partial^4\Phi_{sm}}{\partial x^4}\Psi_{sn} + 2\left(\frac{\partial^2\Phi_{bm}}{\partial x^2}\frac{\partial^2\Psi_{bn}}{\partial y^2} + \frac{\partial^2\Phi_{sm}}{\partial x^2}\frac{\partial^2\Psi_{sn}}{\partial y^2}\right)\right.\\
&\left.+\frac{\partial^4\Psi_{sm}}{\partial y^4}\Phi_{sn} + \frac{\partial^4\Psi_{bm}}{\partial y^4}\Phi_{bn}\right)\Bigg] + k_p\left(1-(ea)^2\left(\frac{\partial}{\partial x^2}+\frac{\partial}{\partial x^2}\right)\right)\\
&\left[\frac{\partial^2\Phi_{bm}}{\partial x^2}\Psi_{bn} + \frac{\partial^2\Phi_{sm}}{\partial x^2}\Psi_{sn} + \frac{\partial^2\Psi_{sm}}{\partial y^2}\Phi_{sn} + \frac{\partial^2\Psi_{bm}}{\partial y^2}\Phi_{bn}\right]\\
&- k_w\left(1-(ea)^2\left(\frac{\partial}{\partial x^2}+\frac{\partial}{\partial x^2}\right)\right)(\Phi_{bm}\Psi_{bn}+\Phi_{sm}\Psi_{sn})\\
&+ \omega^2\frac{4m_c}{ab}\sin^2\left(\pi\frac{x_0}{a}\right)\sin^2\left(\pi\frac{y_0}{b}\right)\left(1-(ea)^2\left(\frac{\partial}{\partial x^2}+\frac{\partial}{\partial x^2}\right)\right)\\
&\cdot(\Phi_{bm}\Psi_{bn}+\Phi_{sm}\Psi_{sn})\Bigg]\,\mathrm{d}x\,\mathrm{d}y = 0,
\end{aligned}\tag{3.5}$$

$$
\begin{aligned}
(3.6)\quad & \int_0^b \int_0^a \varPhi_{sm}\varPsi_{sn}\Bigg[-D_{11}^s\left[\frac{\partial^4\varPhi_{bm}}{\partial x^4}\varPsi_{bn} - l^2\left(\frac{\partial^6\varPhi_{bm}}{\partial x^6}\varPsi_{bn} + \frac{\partial^4\varPhi_{bm}}{\partial x^4}\frac{\partial^2\varPsi_{bn}}{\partial y^2}\right)\right] \\
& - 2(D_{12}^s + 2D_{66}^s)\left[\frac{\partial^2\varPhi_{bm}}{\partial x^2}\frac{\partial^2\varPsi_{bn}}{\partial y^2} - l^2\left(\frac{\partial^4\varPhi_{bm}}{\partial x^4}\frac{\partial^2\varPsi_{bn}}{\partial y^2} + \frac{\partial^2\varPhi_{bm}}{\partial x^2}\frac{\partial^4\varPsi_{bn}}{\partial y^4}\right)\right] \\
& - D_{22}^s\left[\frac{\partial^4\varPsi_{bm}}{\partial y^4}\varPhi_{bn} - l^2\left(\frac{\partial^6\varPsi_{bm}}{\partial y^6}\varPhi_{bn} + \frac{\partial^2\varPhi_{bm}}{\partial x^2}\frac{\partial^4\varPsi_{bn}}{\partial y^4}\right)\right] \\
& - H_{11}^s\left[\frac{\partial^4\varPhi_{sm}}{\partial x^4}\varPsi_{sn} - l^2\left(\frac{\partial^6\varPhi_{sm}}{\partial x^6}\varPsi_{sn} + \frac{\partial^4\varPhi_{sm}}{\partial x^4}\frac{\partial^2\varPsi_{sn}}{\partial y^2}\right)\right] \\
& - 2(H_{12}^s + 2H_{66}^s)\left[\frac{\partial^2\varPhi_{sm}}{\partial x^2}\frac{\partial^2\varPsi_{sn}}{\partial y^2} - l^2\left(\frac{\partial^4\varPhi_{sm}}{\partial x^4}\frac{\partial^2\varPsi_{sn}}{\partial y^2} + \frac{\partial^2\varPhi_{sm}}{\partial x^2}\frac{\partial^4\varPsi_{sn}}{\partial y^4}\right)\right] \\
& - H_{22}^s\left[\frac{\partial^4\varPsi_{sm}}{\partial y^4}\varPhi_{sn} - l^2\left(\frac{\partial^6\varPsi_{sm}}{\partial y^6}\varPhi_{sn} + \frac{\partial^2\varPhi_{sm}}{\partial x^2}\frac{\partial^4\varPsi_{sn}}{\partial y^4}\right)\right] \\
& - (N^T + N^H)\left[\frac{\partial^2\varPhi_{bm}}{\partial x^2}\varPsi_{bn} + \frac{\partial^2\varPhi_{sm}}{\partial x^2}\varPsi_{sn} + \frac{\partial^2\varPsi_{sm}}{\partial y^2}\varPhi_{sn} + \frac{\partial^2\varPsi_{bm}}{\partial y^2}\varPhi_{bn}\right] \\
& - (ea)^2\left[\frac{\partial^4\varPhi_{bm}}{\partial x^4}\varPsi_{bn} + \frac{\partial^4\varPhi_{sm}}{\partial x^4}\varPsi_{sn} + 2\left(\frac{\partial^2\varPhi_{bm}}{\partial x^2}\frac{\partial^2\varPsi_{bn}}{\partial y^2} + \frac{\partial^2\varPhi_{sm}}{\partial x^2}\frac{\partial^2\varPsi_{sn}}{\partial y^2}\right)\right. \\
& \left. + \frac{\partial^4\varPsi_{sm}}{\partial y^4}\varPhi_{sn} + \frac{\partial^4\varPsi_{bm}}{\partial y^4}\varPhi_{bn}\right] + A_{55}^s\left[\frac{\partial^2\varPhi_{sm}}{\partial x^2}\varPsi_{sn} - l^2\left(\frac{\partial^4\varPhi_{sm}}{\partial x^4}\varPsi_{sn} + \frac{\partial^2\varPhi_{sm}}{\partial x^2}\frac{\partial^2\varPsi_{sn}}{\partial y^2}\right)\right] \\
& + A_{44}^s\left[\frac{\partial^2\varPsi_{sm}}{\partial y^2}\varPhi_{sn} - l^2\left(\frac{\partial^4\varPsi_{sm}}{\partial y^4}\varPhi_{sn} + \frac{\partial^2\varPhi_{sm}}{\partial x^2}\frac{\partial^2\varPsi_{sn}}{\partial y^2}\right)\right] \\
& + k_p\left(1 - (ea)^2\left(\frac{\partial}{\partial x^2} + \frac{\partial}{\partial x^2}\right)\right)\left[\frac{\partial^2\varPhi_{bm}}{\partial x^2}\varPsi_{bn} + \frac{\partial^2\varPhi_{sm}}{\partial x^2}\varPsi_{sn} + \frac{\partial^2\varPsi_{sm}}{\partial y^2}\varPhi_{sn} + \frac{\partial^2\varPsi_{bm}}{\partial y^2}\varPhi_{bn}\right] \\
& - k_w\left(1 - (ea)^2\left(\frac{\partial}{\partial x^2} + \frac{\partial}{\partial x^2}\right)\right)(\varPhi_{bm}\varPsi_{bn} + \varPhi_{sm}\varPsi_{sn}) \\
& + \omega^2\frac{4m_c}{ab}\sin^2\left(\pi\frac{x_0}{a}\right)\sin^2\left(\pi\frac{y_0}{b}\right)\left(1 - (ea)^2\left(\frac{\partial}{\partial x^2} + \frac{\partial}{\partial x^2}\right)\right) \\
& (\varPhi_{bm}\varPsi_{bn} + \varPhi_{sm}\varPsi_{sn})\Bigg]\,\mathrm{d}x\,\mathrm{d}y = 0.
\end{aligned}
$$

The function $\varPhi_m$ for different boundary conditions is defined by:

$$
(3.7)\qquad \text{SS:}\quad \varPhi_m(x) = \sin(\lambda_m x), \quad \lambda_m = \frac{m\pi}{a},
$$

$$
\begin{aligned}
(3.8)\qquad \text{CC:}\quad & \varPhi_m(x) = \sin(\lambda_m x) - \sinh(\lambda_m x) - \xi_m(\cos(\lambda_m x) - \cosh(\lambda_m x)), \\
& \xi_m = \frac{\sin(\lambda_m x) - \sinh(\lambda_m x)}{\cos(\lambda_m x) - \cosh(\lambda_m x)}, \qquad \lambda_1 = 4.730, \qquad \lambda_2 = 7.853, \\
& \lambda_3 = 10.996, \qquad \lambda_4 = 14.137, \qquad \lambda_{m\geq 5} = \frac{(m+0.5)\,\pi}{a},
\end{aligned}
$$

$$\text{(3.9)} \quad \text{CS:} \quad \Phi_m(x) = \sin(\lambda_m x) - \sinh(\lambda_m x) - \xi_m(\cos(\lambda_m x) - \cosh(\lambda_m x)),$$
$$\xi_m = \frac{\sin(\lambda_m x) + \sinh(\lambda_m x)}{\cos(\lambda_m x) + \cosh(\lambda_m x)}, \qquad \lambda_1 = 3.927, \qquad \lambda_2 = 7.069,$$
$$\lambda_3 = 10.210, \qquad \lambda_4 = 13.352, \qquad \lambda_{m\geq 5} = \frac{(m+0.25)\,\pi}{a}.$$

The function Ψ_n can be obtained by replacing x, m, and a, respectively by y, n, and b. Setting the coefficient matrix of the above equations leads to the following eigenvalue problem:

$$([K]) \left\{ \begin{array}{c} W_b \\ W_s \end{array} \right\} = 0, \tag{3.10}$$

where $[K]$ is the stiffness matrix. Finally, setting the coefficient matrix to zero gives the buckling loads. It should be noted that calculations are performed based on the following dimensionless quantities:

$$\overline{N} = N\frac{a^2}{D^*}, \qquad \widehat{\omega} = \omega\frac{a^2}{h}\sqrt{\frac{\rho}{E}}, \qquad K_w = k_w\frac{a^4}{D^*}, \qquad K_p = k_p\frac{a^2}{D^*},$$
$$D^* = \frac{Eh^3}{12(1-v^2)}, \qquad \mu = \frac{ea}{a}, \qquad \lambda = \frac{l}{a}. \tag{3.11}$$

4. Numerical results and their discussion

This section is devoted to study the hygro-thermo-mechanical buckling behavior of nonlocal strain gradient bedded graphene sheets-based mass sensors based on a two-variable shear deformation theory. The model introduces two scale coefficients related to nonlocal and strain gradient effects for a more accurate analysis of graphene sheets. Configuration of graphene sheet resting on elastic substrate and distribution of mass sensors are shown in Figs 1 and 2. Material

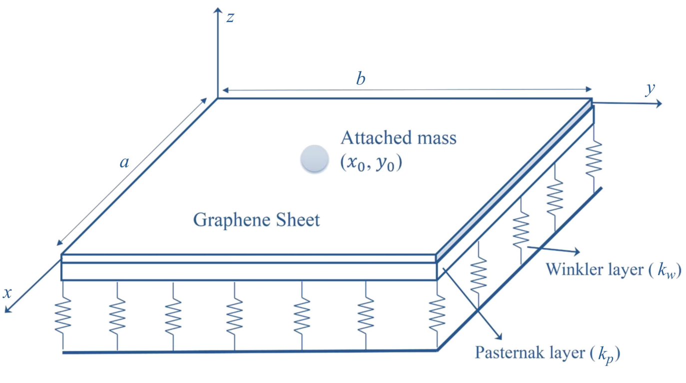

Fig. 1. Configuration of graphene sheet resting on an elastic substrate.

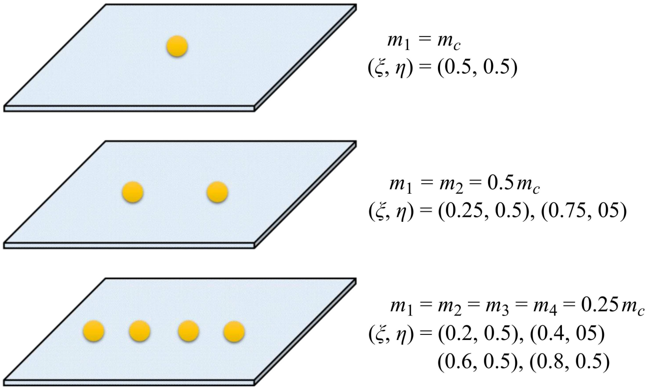

Fig. 2. Distribution of nanoparticles and their mass.

properties of the graphene sheet are: $E = 1$ TPa, $v = 0.19$, and $\rho = 2300$ kg/m^3. Also, the thickness of the graphene sheet is considered as $h = 0.34$ nm. Buckling loads of a nanoplate are validated with those obtained by Hashemi and Samaei [4] for various nonlocal parameters ($\mu = 0$, 0.5, 1, 1.5, 2 nm^2). Obtained buckling loads via the present Galerkin method are in excellent agreement with those of the exact solution presented by Hashemi and Samaei [4], as shown in Table 1. For the comparison study, the strain gradient or length scale parameter and mass sensor are set to zero.

Table 1. Comparison of buckling loads of a graphene sheet for various nonlocal parameters.

μ	$a/h = 100$		$a/h = 20$	
	Hashemi and Samaei [4]	Present	Hashemi and Samaei [4]	Present
0	9.8671	9.86683	9.8067	9.80062
0.5	9.4029	9.40282	9.3455	9.33972
1	8.9803	8.98049	8.9527	8.92023
1.5	8.5939	8.59447	8.5420	8.53680
2	8.2393	8.24026	8.1898	8.18497

Examination of nonlocal and strain gradient effects on buckling loads of graphene sheets for different boundary conditions (SSSS, CSSS, CCSS, and CCCC) is presented in Fig. 3. In this figure, various values of nonlocal parameter ($\mu = 0 \sim 0.5$) and length scale parameter ($\lambda = 0$, 0.1, 0.15, 0.2) are considered. It is clear that when $\lambda = 0$, the buckling loads of a graphene sheet based on a well-known nonlocal elasticity theory will be obtained. However, when both $\mu = 0$ and $\lambda = 0$, the results based on classical continuum mechanics are rendered. It is observed that the buckling load of the graphene sheet reduces with an increase of nonlocal parameter for every kind of boundary condition. This ob-

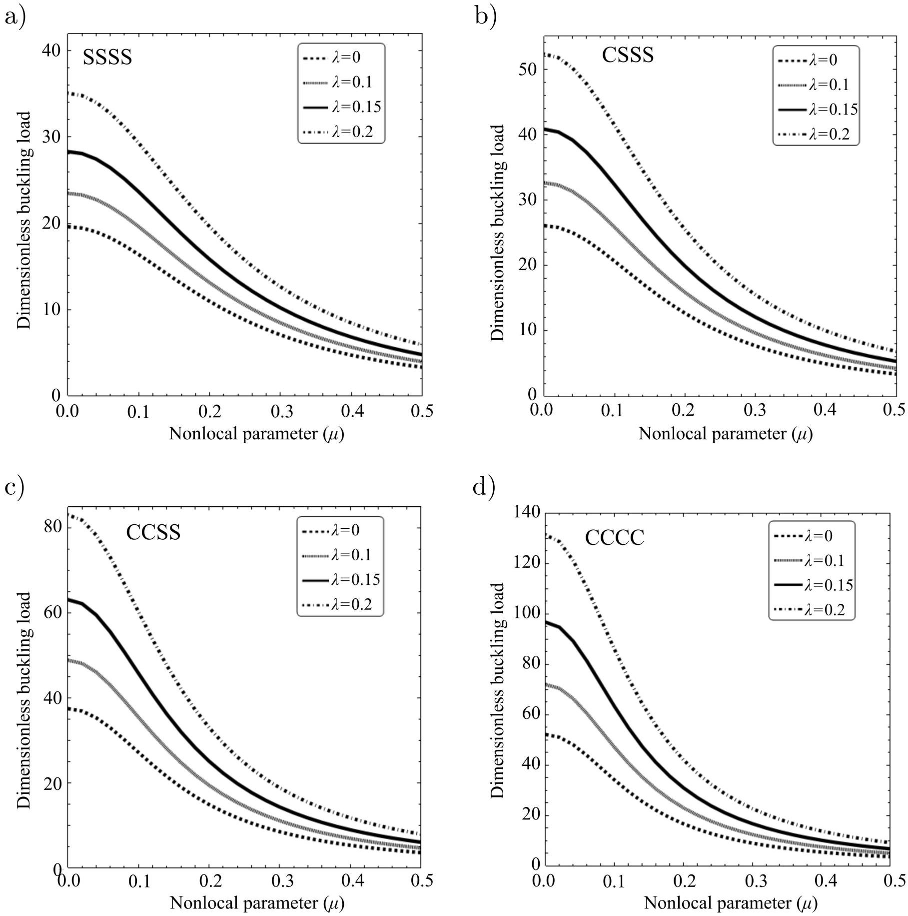

Fig. 3. Variation of the dimensionless buckling load *versus* nonlocal parameter for different length scale parameters and boundary conditions.

servation indicates that the nonlocal parameter exerts a stiffness-softening effect, which leads to lower vibration frequencies. However, the effect of the nonlocal parameter on the magnitude of buckling loads depends on the value of strain gradient or length scale parameter. In fact, the buckling load of the graphene sheet increases with an increase of length scale parameter, which highlights the stiffness-hardening effect due to the strain gradients. Also, it is clear that making the graphene sheet more rigid by increasing the number of clamped edges leads to higher buckling loads.

In Fig. 4, a variation of the dimensionless buckling load of a nonlocal strain gradient graphene sheet ($\mu = 0.2$, $\lambda = 0.1$) *versus* moisture concentration rise for different temperatures ($\Delta T = 0$, 20, 50, 80) and boundary conditions is plotted. It is well-known that hygro-thermal loadings degrade the plate stiffness

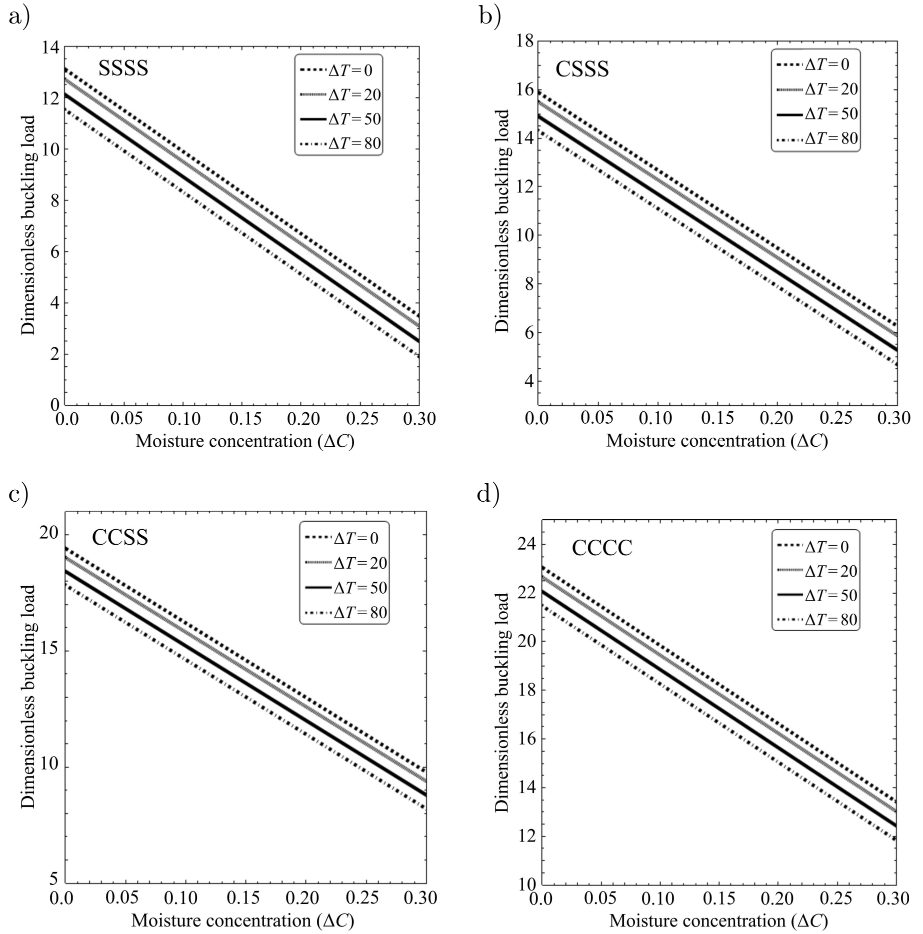

FIG. 4. Variation of the dimensionless buckling load *versus* moisture rise for different temperature changes and boundary conditions ($\mu = 0.2$, $\lambda = 0.1$).

and significantly affect the performance of structures. It is seen that an increase of moisture concentration (ΔC) leads to smaller dimensionless buckling loads for every value of temperature change. However, temperature increase leads to lower buckling loads at a fixed moisture concentration rise. So, the buckling load of a graphene sheet decreases significantly when it is subjected to a severe hygro-thermal environment.

Figure 5 demonstrates the variation of the dimensionless buckling load *versus* length scale parameter for different the Winkler and Pasternak constants when $\mu = 0.2$, $\lambda = 0.1$, $\Delta T = 50$, $\Delta C = 0.1$. However, it is clear that the buckling load of the graphene sheet depends on the values of both Winkler and Pasternak parameters. In fact, the Pasternak layer provides continuous interaction with the graphene sheet, while the Winkler layer has a discontinuous interaction with

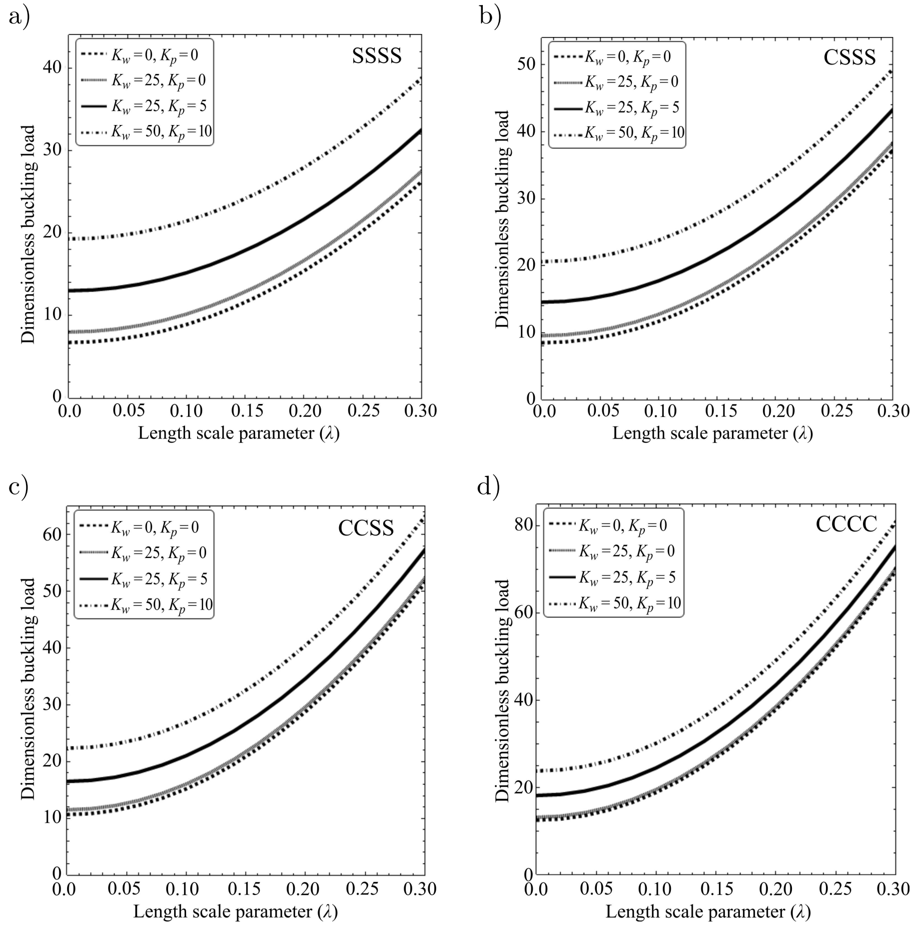

FIG. 5. Variation of the dimensionless buckling load *versus* length scale parameter for different foundation parameters and boundary conditions ($\mu = 0.2$, $\lambda = 0.1$, $\Delta T = 50$, $\Delta C = 0.1$).

the graphene sheet. Increasing the Winkler and Pasternak parameters leads to larger buckling loads by enhancing the bending rigidity of graphene sheets. But, the Pasternak layer shows more increasing effect on buckling loads compared with the Winkler layer. It is found that the magnitude of buckling load for various values of foundation parameters depends on the strain gradient effect. As previously mentioned, increasing the length scale parameter leads to larger buckling loads for every value of foundation parameters.

Figure 6 illustrates the variation of dimensionless frequency of graphene sheet *versus* nanoparticle mass for various foundation parameters and nanoparticle location at $\mu = 0.2$ and $\lambda = 0.1$. It is seen that for every location of nanoparticle, increasing its mass leads to reduction in vibration frequencies. One can also see that the variation of frequency is apparent when the attached mass is

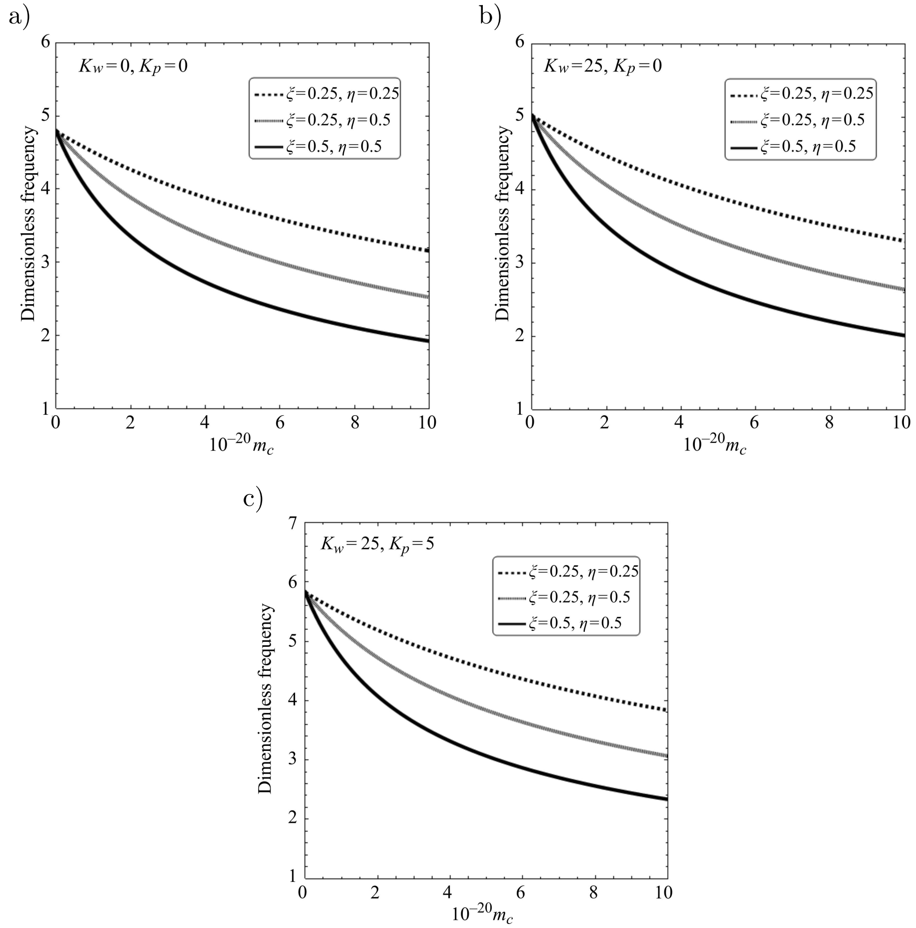

Fig. 6. Dimensionless frequency of graphene sheet *versus* nanoparticle mass for various foundation parameters and nanoparticle location ($\mu = 0.2$, $\lambda = 0.1$).

larger than 10^{-21} g. In fact, the mass sensitivity of the nanomechanical mass sensor can reach at least 10^{-21} g. Also, it is found that the effect of nanoparticle location becomes more prominent as the attached mass increases. As the nanoparticle becomes closer to the plate center, the vibration frequency of the nanomechanical mass sensor reduces. It is also clear that the vibration behavior of the nanomechanical mass sensor depends on the values of both the Winkler and Pasternak parameters. In fact, the Pasternak layer provides continuous interaction with the graphene sheet, while the Winkler layer has a discontinuous interaction with the graphene sheet. Increasing the Winkler and Pasternak parameters leads to larger frequencies by enhancing the bending rigidity of graphene sheets. But, the Pasternak layer shows more increasing effect on the frequencies compared with the Winkler layer. Figure 7 depicts the variation of

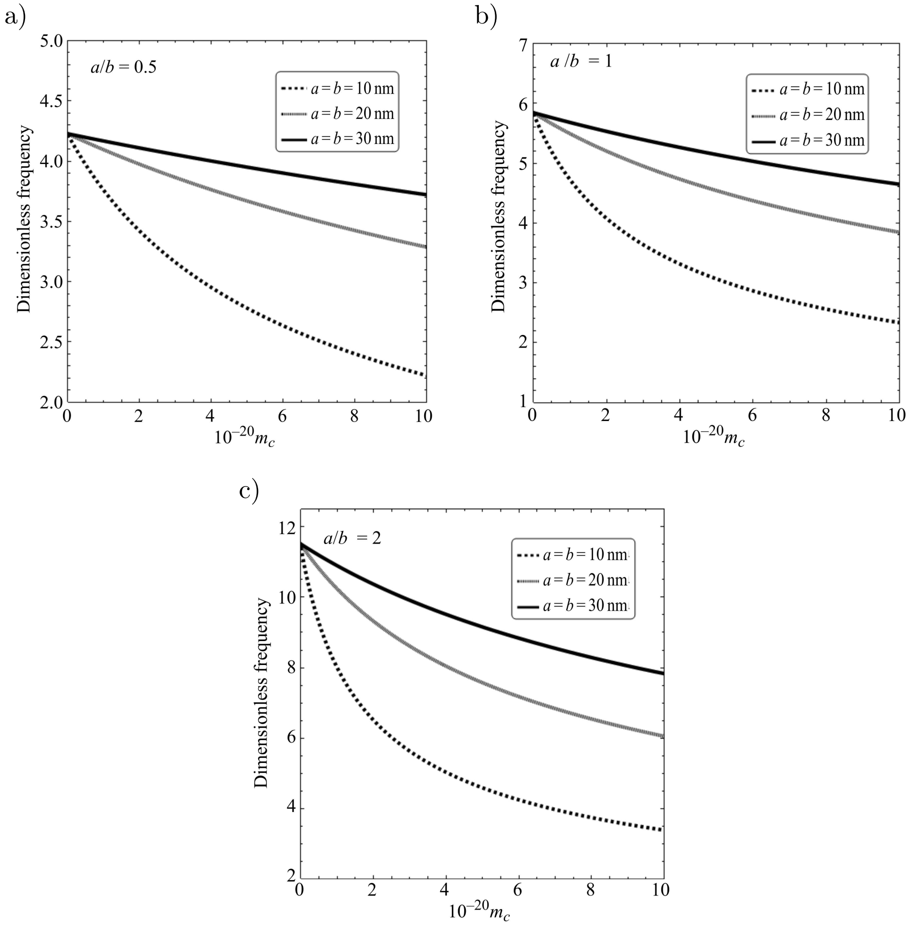

FIG. 7. Dimensionless frequency of graphene sheet *versus* nanoparticle mass for various aspect ratios ($\mu = 0.2$, $\lambda = 0.1$, $K_w = 25$, $K_p = 5$).

dimensionless frequency *versus* attached mass for different length and width parameters and aspect ratios (a/b) at $K_w = 25$, $K_p = 5$, $\mu = 0.2$, $\lambda = 0.1$. It is seen that graphene sheets with higher lengths have larger vibration frequencies. This is because graphene sheets with smaller sizes are more rigid. So, a graphene sheet mass sensor with smaller sizes is more sensitive to the attached mass. In fact, variation of the dimensionless frequency with respect to the attached mass becomes more significant as the graphene sheet size reduces.

Magnetic field effect on vibration frequency of the nano-mechanical mass sensor with respect to the attached mass for different scale parameters is presented in Fig. 8 at $K_w = 25$, $K_p = 5$. It must be noted that in-plane magnetic field has a stiffness-hardening impact on the graphene sheet. In fact, increase of magnetic field intensity leads to large frequencies. As a conclusion, in-plane magnetic field

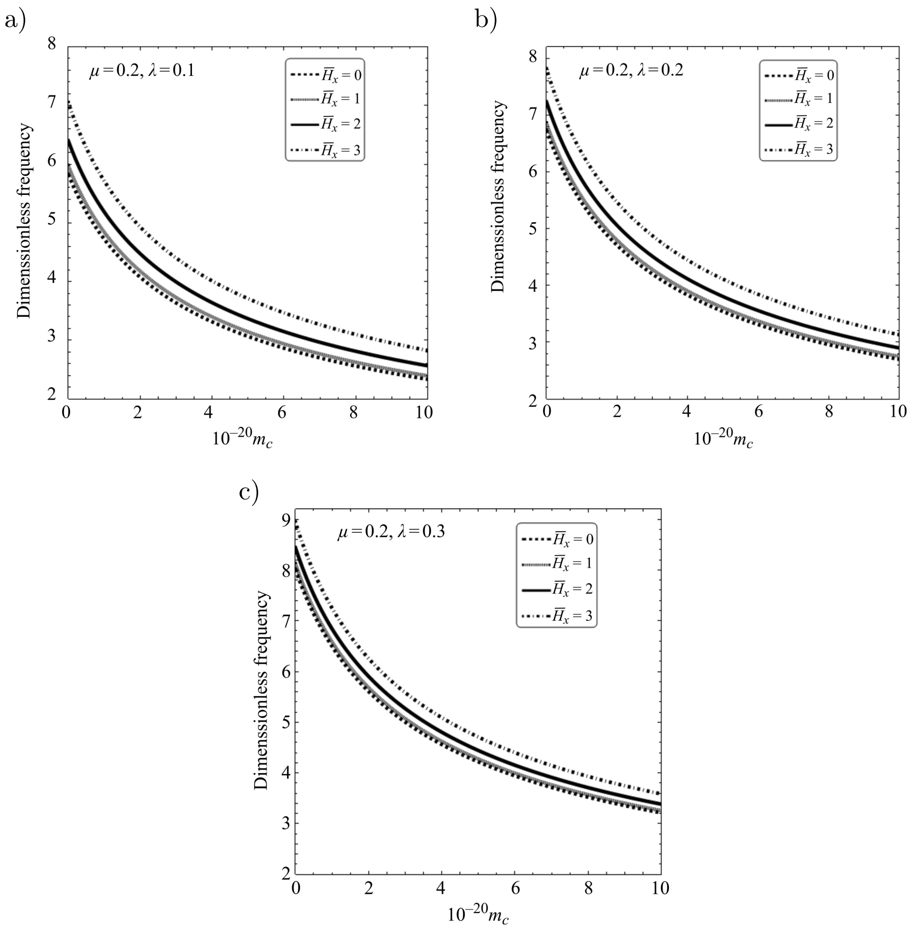

FIG. 8. Dimensionless frequency of graphene sheet *versus* nanoparticle mass for various magnetic fields.

has a major role on the vibration behavior of nano-mechanical mass sensor and should be checked for their accurate design.

5. Conclusions

In this paper, the nonlocal strain gradient theory was employed to investigate the buckling behavior of single-layer graphene sheets in the hygro-thermal environment resting on the elastic medium using a refined two-variable plate theory. The theory introduces two scale parameters corresponding to nonlocal and strain gradient effects to capture both stiffness-softening and stiffness-hardening influences. Hamilton's principle was employed to obtain the governing equation of a nonlocal strain gradient graphene sheet. These equations were solved via

Galerkin's method to obtain the buckling loads. It is observed that the buckling load of the graphene sheet reduced with the increase of the nonlocal parameter. In contrast, the buckling load increased with an increase of the length scale parameter, which highlights the stiffness-hardening effect due to the strain gradients. Also, the increase of temperature and moisture degraded the plate stiffness and the buckling loads reduces. All these observations are affected by the number of attached nanoparticles and their mass. However, as the nanoparticle became closer to the plate center, the vibration frequency of the nanomechanical mass sensor reduced.

Acknowledgements

The author conveys his sincere thanks to Karunya Institute of Technology and Sciences, Coimbatore, India, for providing financial assistance through KSTG seed money. Also, he is grateful to the reviewers for their wise suggestions.

References

1. Lim C.W., Zhang G., Reddy J.N., A higher-order nonlocal elasticity and strain gradient theory and its applications in wave propagation, *Journal of the Mechanics and Physics of Solids*, **78**: 298–313, 2015, doi: 10.1016/j.jmps.2015.02.001.

2. Eringen A.C., Edelen D.G.B., On nonlocal elasticity, *International Journal of Engineering Science*, **10**(3): 233–248, 1972, doi: 10.1016/0020-7225(72)90039-0.

3. Eringen A.C., On differential equations of nonlocal elasticity and solutions of screw dislocation and surface waves, *International Journal of Applied Physics*, **54**(9): 4703–4710, 1983, doi: 10.1063/1.332803.

4. Hashemi S.H., Samaei A.T., Buckling analysis of micro/nanoscale plates via nonlocal elasticity theory, *Physica E: Low-dimensional Systems and Nanostructures*, **43**(7): 1400–1404, 2011, doi: 10.1016/j.physe.2011.03.012.

5. Kheroubi B., Benzair A., Tounsi A., Semmah A., A new refined nonlocal beam theory accounting for effect of thickness stretching in nanoscale beams, *Advances in Nano Research*, **4**(4): 251–264, 2016, doi: 10.12989/anr.2016.4.4.251.

6. Ebrahimi F., Daman M., Analytical investigation of the surface effects on nonlocal vibration behavior of nanosize curved beams, *Advances in Nano Research*, **5**(1): 35–47, 2017, doi: 10.12989/anr.2017.5.1.035.

7. Rakrak K., Zidour M., Heireche H., Bousahla A.A., Chemi A., Free vibration analysis of chiral double-walled carbon nanotube using non-local elasticity theory, *Advances in Nano Research*, **4**(1): 31–44, 2016, doi: 10.12989/anr.2016.4.1.031.

8. Aydogdu M., Arda M., Filiz S., Vibration of axially functionally graded nano rods and beams with a variable nonlocal parameter, *Advances in Nano Research*, **6**(3): 257–278, 2018, doi: 10.12989/anr.2018.6.3.257.

9. Elmerabet A.H., Heireche H., Tounsi A., Semmah A., Buckling temperature of a single-walled boron nitride nanotubes using a novel nonlocal beam model, *Advances in Nano Research*, **5**(1): 1–12, 2017, doi: 10.12989/anr.2017.5.1.001.

10. Pradhan S.C., Murmu T., Small scale effect on the buckling of single-layered graphene sheets under biaxial compression via nonlocal continuum mechanics, *Computational Materials Science*, **47**(1): 268–274, 2009, doi: 10.1016/j.commatsci.2009.08.001.

11. Pradhan S.C., Kumar A., Vibration analysis of orthotropic graphene sheets using nonlocal elasticity theory and differential quadrature method, *Composite Structures*, **93**(2): 774–779, 2011, doi: 10.1016/j.compstruct.2010.08.004.

12. Aksencer T., Aydogdu M., Levy type solution method for vibration and buckling of nanoplates using nonlocal elasticity theory, *Physica E: Low-dimensional Systems and Nanostructures*, **43**(4), 954–959, 2011, doi: 10.1016/j.physe.2010.11.024.

13. Mohammadi M., Farajpour A., Moradi A., Ghayour M., Shear buckling of orthotropic rectangular graphene sheet embedded in an elastic medium in thermal environment, *Composites Part B: Engineering*, **56**: 629–637, 2014, doi: 10.1016/j.compositesb.2013.08.060.

14. Mohammadi M., Goodarzi M., Ghayour M., Farajpour A., Influence of in-plane pre-load on the vibration frequency of circular graphene sheet via nonlocal continuum theory, *Composites Part B: Engineering*, **51**: 121–129, 2013, doi: 10.1016/j.compositesb.2013.02.044.

15. Ansari R., Arash B., Rouhi H., Vibration characteristics of embedded multi-layered graphene sheets with different boundary conditions via nonlocal elasticity, *Composite Structures*, **93**(9): 2419–2429, 2011, doi: 10.1016/j.compstruct.2011.04.006.

16. Shen Z-B., Tang H-L., Li D-K., Tang G-J., Vibration of single-layered graphene sheet-based nanomechanical sensor via nonlocal Kirchhoff plate theory, *Computational Materials Science*, **61**: 200–205, 2012, doi: 10.1016/j.commatsci.2012.04.003.

17. Farajpour A., Shahidi A.R., Mohammadi M., Mahzoon M., Buckling of orthotropic micro/nanoscale plates under linearly varying in-plane load via nonlocal continuum mechanics, *Composite Structures*, **94**(5): 1605–1615, 2012, doi: 10.1016/j.compstruct.2011.12.032.

18. Ansari R., Sahmani S., Prediction of biaxial buckling behavior of single-layered graphene sheets based on nonlocal plate models and molecular dynamics simulations, *Applied Mathematical Modelling*, **37**(12–13): 7338–7351, 2013, doi: 10.1016/j.apm.2013.03.004.

19. Sobhy M., Thermomechanical bending and free vibration of single-layered graphene sheets embedded in an elastic medium, *Physica E: Low-dimensional Systems and Nanostructures*, **56**: 400–409, 2014, doi: 10.1016/j.physe.2013.10.017.

20. Ebrahimi F., Barati M.R., An exact solution for buckling analysis of embedded piezo-electro-magnetically actuated nanoscale beams, *Advances in Nano Research*, **4**(2): 65–84, 2016, doi: 10.12989/anr.2016.4.2.065.

21. Ehyaei J., Daman M., Free vibration analysis of double walled carbon nanotubes embedded in an elastic medium with initial imperfection, *Advances in Nano Research*, **5**(2): 179–192, 2017, doi: 10.12989/anr.2017.5.2.179.

22. Narendar S., Gopalakrishnan S., Scale effects on buckling analysis of orthotropic nanoplates based on nonlocal two-variable refined plate theory, *Acta Mechanica*, **223**(2): 395–413, 2012, doi: 10.1007/s00707-011-0560-5.

23. Murmu T., Mccarthy M. A., Adhikari S., In-plane magnetic field affected transverse vibration of embedded single-layer graphene sheets using equivalent nonlocal elasticity approach, *Composite Structures*, **96**: 57–63, 2013, doi: 10.1016/j.compstruct.2012.09.005.

24. Bessaim A., Houari M.S.A., Bernard F., Tounsi A., A nonlocal quasi-3D trigonometric plate model for free vibration behaviour of micro/nanoscale plates, *Structural Engineering and Mechanics*, **56**(2): 223–240, 2015, doi: 10.12989/sem.2015.56.2.223.

25. Hashemi S.H., Mehrabani H., Ahmadi-Savadkoohi A., Exact solution for free vibration of coupled double viscoelastic graphene sheets by viscoPasternak medium, *Composites Part B: Engineering*, **78**: 377–383, 2015, doi: 10.1016/j.compositesb.2015.04.008.

26. Ebrahimi F., Shafiei N., Influence of initial shear stress on the vibration behavior of single-layered graphene sheets embedded in an elastic medium based on Reddy's higher-order shear deformation plate theory, *Mechanics of Advanced Materials and Structures*, **24**(9): 761–772, 2016, doi: 10.1080/15376494.2016.1196781.

27. Jiang R.W., Shen Z.B., Tang G.J., Vibration analysis of a single-layered graphene sheet-based mass sensor using the Galerkin strip distributed transfer function method, *Acta Mechanica*, **227**(10): 2899–2910, 2016, doi: 10.1007/s00707-016-1649-7.

28. Arani A.G., Haghparast E., Zarei H.B., Nonlocal vibration of axially moving graphene sheet resting on orthotropic visco-Pasternak foundation under longitudinal magnetic field, *Physica B: Condensed Matter*, **495**: 35–49, 2016, doi: 10.1016/j.physb.2016.04.039.

29. Aslanyan N.S., Sargsyan S.H., Applied theories of thermoelasticity of micropolar thin beams, *Journal of Thermal Stresses*, **41**(6): 687–705, 2018, doi: 10.1080/01495739.2018.1426066.

30. Bachiri A., Bourada M., Mahmoudi A., Benyoucef S., Tounsi A., Thermodynamic effect on the bending response of elastic foundation FG plate by using a novel four variable refined plate theory, *Journal of Thermal Stresses*, **41**(8): 1042–1062, 2018, doi: 10.1080/01495739.2018.1452169.

31. Cinefra M., Petrolo M., Li G., Carrera E., Variable kinematic shell elements for composite laminates accounting for hygrothermal effects, *Journal of Thermal Stresses*, **40**(12): 1523–1544, 2017, doi: 10.1080/01495739.2017.1360165.

32. Jaiani G., Bitsadze L., Basic problems of thermoelasticity with microtemperatures for the half-space, *Journal of Thermal Stresses*, **41**(9): 1101–1114, 2018, doi: 10.1080/01495739.2018.1464415.

33. Khdeir A.A., Thermoelastic response of cross-ply laminated shells based on a rigorous shell theory, *Journal of Thermal Stresses*, **35**(11): 1000–1017, 2012, doi: 10.1080/01495739.2012.720219.

34. Mirzaei M., Thermal buckling of temperature-dependent composite super elliptical plates reinforced with carbon nanotubes, *Journal of Thermal Stresses*, **41**(7): 920–935, 2018, doi: 10.1080/01495739.2018.1429969.

35. Vinyas M., Kattimani S.C., Joladarashi S., Hygrothermal coupling analysis of magneto-electroelastic beams using finite element methods, *Journal of Thermal Stresses*, **41**(8): 1063–1079, 2018, doi: 10.1080/01495739.2018.1447856.

36. Kurtinaitiene M., Mazeika K., Ramanavicius S., Pakstas V., Jagminas A., Effect of additives on the hydrothermal synthesis of manganese ferrite nanoparticles, *Advances in Nano Research*, **4**(1): 1–14, 2016, doi: 10.12989/anr.2016.4.1.001.

37. Ebrahimi F., Babaei R., Shaghaghi G.R., Vibration analysis thermally affected viscoelastic nanosensors subjected to linear varying loads, *Advances in Nano Research*, **6**(4): 399–422, 2018, doi: 10.12989/anr.2018.6.4.399.

38. Ebrahimi F., Habibi S., Low-velocity impact response of laminated FG-CNT reinforced composite plates in thermal environment, *Advances in Nano Research*, **5**(2): 69–97, 2017, doi: 10.12989/anr.2018.6.4.399.

39. Sobhy M., Hygrothermal vibration of orthotropic double-layered graphene sheets embedded in an elastic medium using the two-variable plate theory, *Applied Mathematical Modelling*, **40**(1): 85–99, 2016, doi: 10.1016/j.apm.2015.04.037.

40. Zenkour A.M., Nonlocal transient thermal analysis of a single-layered graphene sheet embedded in viscoelastic medium, *Physica E: Low-dimensional Systems and Nanostructures*, **79**: 87–97, 2016, doi: 10.1016/j.physe.2015.12.003.

41. Aydogdu M., Filiz S., Modeling carbon nanotube-based mass sensors using axial vibration and nonlocal elasticity, *Physica E: Low-dimensional Systems and Nanostructures*, **43**(6): 1229–1234, 2011, doi: 10.1016/j.physe.2011.02.006.

42. Sakhaee-Pour A., Ahmadian M.T., Vafai A., Applications of single-layered graphene sheets as mass sensors and atomistic dust detectors, *Solid State Communications*, **145**(4): 168–172, 2008, doi: 10.1016/j.ssc.2007.10.032.

43. Lam D.C.C., Yang F., Chong A.C.M., Wang J., Tong P., Experiments and theory in strain gradient elasticity, *Journal of the Mechanics and Physics of Solids*, **51**(8): 1477–1508, 2003, doi: 10.1016/S0022-5096(03)00053-X.

44. Li L., Hu Y., Wave propagation in fluid-conveying viscoelastic carbon nanotubes based on nonlocal strain gradient theory, *Computational Materials Science*, **112**(Part A): 282–288, 2016, doi: 10.1016/j.commatsci.2015.10.044.

45. Li L., Hu Y., Li X., Longitudinal vibration of size-dependent rods via nonlocal strain gradient theory, *International Journal of Mechanical Sciences*, **115–116**: 135–144, 2016, doi: 10.1016/j.ijmecsci.2016.06.011.

46. Ebrahimi F., Barati M.R., Vibration analysis of nonlocal beams made of functionally graded material in thermal environment, *The European Physical Journal Plus*, **131**(8): 279, 2016, doi: 10.1140/epjp/i2016-16279-y.

47. Ebrahimi F., Barati M.R., A unified formulation for dynamic analysis of nonlocal heterogeneous nanobeams in hygro-thermal environment, *Applied Physics A*, **122**(9): 792, 2016, doi: 10.1007/s00339-016-0322-2.

48. Ebrahimi F., Barati M.R., A nonlocal higher-order refined magneto-electro-viscoelastic beam model for dynamic analysis of smart nanostructures, *International Journal of Engineering Science*, **107**: 183–196, 2016, doi: 10.1016/j.ijengsci.2016.08.001.

49. EBRAHIMI F., BARATI M.R., Hygrothermal buckling analysis of magnetically actuated embedded higher order functionally graded nanoscale beams considering the neutral surface position, *Journal of Thermal Stresses*, **39**(10): 1210–1229, 2016, doi: 10.1080/01495739.2016.1215726.

50. EBRAHIMI F., BARATI M.R., Vibration analysis of smart piezoelectrically actuated nanobeams subjected to magneto-electrical field in thermal environment, *Journal of Vibration and Control*, **24**(3): 549–564, 2018, doi: 10.1177/1077546316646239.

51. EBRAHIMI F., BARATI M.R., Static stability analysis of smart magneto-electro-elastic heterogeneous nanoplates embedded in an elastic medium based on a four-variable refined plate theory, *Smart Materials and Structures*, **25**(10): 105014, 2016, doi: 10.1088/0964-1726/25/10/105014.

52. EBRAHIMI F., BARATI M.R., Size-dependent dynamic modeling of inhomogeneous curved nanobeams embedded in elastic medium based on nonlocal strain gradient theory, *Proceedings of the Institution of Mechanical Engineers, Part C: Journal of Mechanical Engineering Science*, **231**(23): 4457–4469, 2017, doi: 10.1177/0954406216668912.

53. EBRAHIMI F., BARATI M.R., Hygrothermal effects on vibration characteristics of viscoelastic FG nanobeams based on nonlocal strain gradient theory, *Composite Structures*, **159**: 433–444, 2017, doi: 10.1016/j.compstruct.2016.09.092.

54. EBRAHIMI F., BARATI M.R., A nonlocal strain gradient refined beam model for buckling analysis of size-dependent shear-deformable curved FG nanobeams, *Composite Structures*, **159**: 174–182, 2017, doi: 10.1016/j.compstruct.2016.09.058.

55. EBRAHIMI F., BARATI M.R., DABBAGH A., A nonlocal strain gradient theory for wave propagation analysis in temperature-dependent inhomogeneous nanoplates, *International Journal of Engineering Science*, **107**: 169–182, 2016, doi: 10.1016/j.ijengsci.2016.07.008.

56. EBRAHIMI F., BARATI M.R., Wave propagation analysis of quasi-3D FG nanobeams in thermal environment based on nonlocal strain gradient theory, *Applied Physics A*, **122**(9): 843, 2016, doi: 10.1007/s00339-016-0368-1.

57. EBRAHIMI F., JAFARI A., SELVAMANI R., Thermal buckling analysis of magneto electro elastic porous FG beam in thermal environment, *Advances in Nano Research*, **8**(1): 83–94, 2020, doi: 10.12989/anr.2020.8.1.083.

58. EBRAHIMI F., KARIMIASL M., SELVAMANI R., Bending analysis of magneto-electro piezoelectric nanobeams system under hygro-thermal loading, *Advances in Nano Research*, **8**(3): 203–214, 2020, doi: 10.12989/anr.2020.8.3.203.

59. EBRAHIMI F., KOKABA M., SHAGHAGHI G., SELVAMANI R., Dynamic characteristics of hygro-magneto-thermo-electrical nanobeam with non-ideal boundary conditions, *Advances in Nano Research*, **8**(2): 169–182, 2020, doi: 10.12989/anr.2020.8.2.169.

60. EBRAHIMI F., HOSSEINI S.H.S., SELVAMANI R., Thermo-electro-elastic nonlinear stability analysis of viscoelastic double-piezo nanoplates under magnetic field, *Structural Engineering and Mechanics*, **73**(5): 565–584, 2020, doi: 10.12989/sem.2020.73.5.565.

61. SELVAMANI R., EBRAHIMI F., Axisymmetric vibration in a submerged, piezoelectric rod coated with thin film, [in:] *Applied Mathematics and Scientific Computing. International Conference on Advances in Mathematical Sciences, Vellore, India, December 2017* – Vol. II, Book Series: *Trends in Mathematics*, B. Rushi Kumar, R. Sivaraj, B.S.R.V. Prasad,

M. Nalliah, A. Subramanyam Reddy [Eds.], Springer International Publishing, 2019, doi: 10.1007/978-3-030-01123-9_21.

62. Ebrahimi F., Salari E., Thermo-mechanical vibration analysis of a single-walled carbon nanotube embedded in an elastic medium based on higher-order shear deformation beam theory, *Journal of Mechanical Science and Technology*, **29**(9): 3797–3803, 2015.

Received May 2, 2020; accepted version July 8, 2020.